A NEW KAOLIN DEPOSIT IN WESTERN AFRICA: MINERALOGICAL AND COMPOSITIONAL FEATURES OF KAOLINITE FROM CALUQUEMBE (ANGOLA)

ESPERANÇA TAULER[1], JINGYAO XU[1*], MARC CAMPENY [1,2], SANDRA AMORES[1], JOAN CARLES MELGAREJO[1], SALVADOR MARTINEZ[1] AND ANTONIO O. GONÇALVES[3]

[1] Departament de Mineralogia, Petrologia i Geologia Aplicada, Facultat de Ciències de la Terra, Universitat de Barcelona, Barcelona, Spain

[2] Departament de Mineralogia, Museu de Ciències Naturals de Barcelona, Barcelona, Spain

[3] Departamento de Geologia, Universidade Agostinho Neto, Luanda, Angola

* e-mail: jingyao.xu@ub.edu

Abstract - Large kaolin deposits developed by weathering on Precambrian granitic rocks have been discovered in the Caluquembe area, Huíla province, Angola. To determine accuracy of analysis and to evaluate the samples kaolinite grade, it was used full profile Rietveld refinement by X-Ray Powder Diffraction (XRPD) and Gravimetric Thermal Analysis (TGA). Caluquembe kaolin is mainly comprised of kaolinite (44 to 93 wt. %), quartz (0 to 23 wt. %) and feldspar (4 to 14 wt. %). AGFI Crystallinity Index, calculated by XRPD profile refinement, indicates low and medium defect kaolinite. Kaolinite particles show a platy habit and they are stacked together forming 'booklets' or radial aggregates, also occurring as fine anhedral particles in a finer-grained mass. Muscovite-kaolinite intergrowths have also been found. Whole-rock chemical composition was analyzed, including major, trace, and Rare Earth Elements (REE). Chondrite and Upper Continental Crust normalized REE patterns show the same tendency for all samples, with a significant enrichment in Light Rare Earth Elements (LREE). Mineralogical and compositional features of the Caluquembe kaolin indicate that it is a suitable material in the manufacture of structural products, such as bricks, pavers and roofing tiles. In addition, REE significant contents of the Caluquembe kaolin can be considered as a potential future target of mining exploration.

Key Words: Caluquembe, Angola, kaolinite, AGFI, REE.

INTRODUCTION

Kaolinite $Al_2Si_2O_5(OH)_4$ is a clay mineral, structurally classified as 1:1 layer type, with a crystalline structure comprised of tetrahedral and octahedral sheets (Young and Hewat, 1988; Moore and Reynolds, 1997; Bish, 1993). It belongs to the spatial group $C\bar{1}$ with a= 5.154 Å, b= 8.942 Å, c= 7.402 Å, α= 91.69°, ß= 104.61° and ɣ=89.92° (Bish, 1993).

Kaolinite is classified within the kaolin subgroup, which also includes other minerals such as dickite, nacrite and a hydrated form of halloysite (Guggenheim *et al*., 2006). Structural differences between these mineral phases are based on their interlayer shift and the location of the octahedral vacancy in successive layers (Bailey, 1980).

Kaolinite is a valuable and versatile industrial mineral with classical applications in the production of bricks, ceramics, paint coatings, paper, and plastic. It also has relatively new applications in catalysis and organic reactivity as well as in the pharmaceutical industry, where it is used in the design of clay-polymer nanocomposites and films (Heckroodt, 1991; Murray, 1999c; Murray, 2000; Detellier and Schoonheydt, 2014; Phipps, 2014; Pruett, 2016; Dedzo and Detellier, 2016; Nguie *et al*., 2016; Mansa *et al*., 2017).

In 2015, world kaolinite production was around 34 million tons (Mt), mainly led by the United States, Germany, Czech Republic and China, among other countries (Flanagan, 2016).

Kaolin deposits are classified as primary, secondary, or tertiary depending on their parent lithology and corresponding alteration processes (Dill, 2016). In primary deposits, the parent lithology is a feldspar-rich magmatic rock – mainly granitic or acid volcanic – and the formation of kaolinite is related to feldspar alteration due to hydrothermal fluid circulation and/or the development of weathering processes (Schroeder and Erickson, 2014). On the other hand, sedimentary processes generate secondary deposits, mainly comprised of detrital clays (Schroeder and Erickson, 2014). Tertiary deposits are generated by very low regional metamorphism developed in argillaceous sediments or sands (Dill, 2016).

Angola has significant and large mineral resources. However, for more than forty years, the Angolan independence and civil wars (1961 – 2002) prevented systematic mining exploration in the country. Nowadays, known mineral resources in Angola include: beryllium, clays, copper, gold, gypsum, iron, lead, lignite, manganese, mica, nickel, phosphates, silver, tungsten, uranium, vanadium and zinc, among others (Bermúdez-Lugo, 2014). However, diamonds are the most economically relevant mineral resource in the country and account for about 5% of worldwide production.

In the case of kaolin, significant deposits have been documented in several regions in Angola (Ekosse, 2010). Most of them are related to weathering of anorthosites from the Kunene anorthositic complex, but systematic studies of these kaolin deposits are still very scarce. The only significant studies were carried out by Gomes *et al*. (1994) and Saviano *et al*. (2005) in the Mevaiela kaolin deposit, located near the village of Quihita in SE Angola.

In the Caluquembe area (Huíla province, Angola), (Fig. 1) extensive kaolin outcrops associated to weathering of Eburnean granitic rocks were recently discovered. This study presents the most relevant mineralogical and compositional features of Caluquembe kaolinite. It has been determined the kaolinite grade of the deposit by processing XRPD spectra using full profile Rietveld refinement and testing the accuracy of the results by TGA. This study also includes kaolin major and trace elements compositions, with especial interest in the distribution of Rare Earth Elements (REE), considering that a significant number of REE deposits worldwide are related to weathering of granitic rocks (Nyakairu and Koeberl, 2001; Nyakairu *et al*., 2001; Njoya *et al*., 2006; Bao and Zhao, 2008; Galán *et al*., 2016; Sanematsu and Watanabe, 2016) or from sedimentary rocks (Kadir and Kart, 2009; Elliott *et al*., 2018). The results obtained may be considered as preliminary evaluation guidelines for future mining exploration of kaolin and accessory REE's in the Caluquembe area.

GEOLOGICAL SETTING

The Caluquembe area is located in the Huíla province (SW Angola), approximately 180 km NE from Lubango and 570 km SE of Luanda, Angola's capital (Fig.1).

Angola's structural framework is generally represented by the Kasai and Congo cratons, which correspond to continental blocks stabilized during the Mesoproterozoic orogeny (Hanson, 2003; Jelsma *et al*., 2011).

The southwestern part of the Congo Craton comprises the Angolan Shield where the occurrence of widespread Paleoproterozoic crust – dominated by granitoids – has been identified together with a limited amount of Archaean crust (de Carvalho *et al*., 2000; McCourt *et al*., 2013) (Figure 1a).. This basement terrane is intruded by the anorthositic Kunene Complex (Ashwal and Twist, 1994; Mayer *et al*., 2004), a set of Mesoproterozoic red granites, and it is also unconformably overlain by supracrustal sequences.

The Caluquembe region is located in one of the four broad tectonic domains that form the Angolan Shield, known as the Central Eburnean Zone (de Carvalho *et al*., 2000; Jelsma *et al*., 2011; McCourt *et al*., 2013). In this domain, paleoproterozoic granitoids are the dominant lithologies (Figure 1). However, more recent lithologies such as Eburnean granitoids linked to the Namib thermotectonic event are also found outcropping in this area (de Carvalho *et al*., 2000). The predominant lithology in the sampled Caluquembe area is the regional Chicala alkaline granite (c. 1700-1650 Ma), outcropping in association with porphyritic granites and other Eburnean granites such as the Yuabre and Quibala granites (Figure 1). Hypabyssal rocks such as dolerites, norites, and olivine basalts also occur across the region – related to anorogenic magmatism that occurred in the middle and late Proterozoic and also towards the end of the Cretaceous, during the Wealdenian reactivation of the Angolan platform (c. 130-100 Ma, Silva and Simões, 1980/1981).

Strong erosion processes were developed during the Cenozoic, accompanied by intense weathering under semi-tropical climatic conditions (Marques, 1977). The alteration of granitic rocks was directly related to the formation of kaolinite weathering profiles.

SAMPLING and METHODS

In the present work, were studied a set of 34 samples obtained in extensive weathering profiles developed on granitic rocks in the Caluquembe region (Figure 2). The studied area is around 20 km^2 and sampling was mainly focused on the available outcrops located along river margins.

The morphology and microtextural features of the studied kaolin samples were examined on polished thin sections with a Nikon Eclipse LV100 POL microscope and an ESEM Quanta 200 FEI, XTE 325/D8395 scanning electron microscope with energy dispersive X-ray spectroscopy (SEM-EDS) at the Scientific and Technological Centers of the University of Barcelona (CCiTUB) (Barcelona, Catalonia, Spain).

Particle size was measured with a Beckman Coulter LS Particle Size Analyzer. To avoid sample flocculation and consequent erroneous measure of grain size distribution, approximately 0.5 grams of dry sample were diluted in a dispersing solution of sodium polyphosphate during 15 minutes using ultrasonic bath. Before the analysis the obtained solution was agitated during 24 hours. This preparation was carried out in Department of Earth and Ocean Dynamics from the Earth Sciences Faculty of the University of Barcelona (Barcelona, Catalonia, Spain).

Microprobe analyses (EMPA) were performed over selected areas on representative polished thin sections. Analyses were carried out with a JEOL JXA-8230 at the CCiTUB. Analytical conditions were a low voltage of 20 kV (in order to excite the weaker lines K, L of certain heavy elements those can present spectral interferences), 10 nA beam current, 2 µm beam diameter and counting time of 10 seconds per element.

Kaolin samples, after dried, were crushed for X-ray Powder Diffraction (XRPD) and Thermal analyses (DTA-TGA) only using agate mortar.

XRPD data were collected with a Panalytical X'Pert PRO MPD X-ray diffractometer with monochromatized incident Cu $K_{\alpha 1}$ radiation at 45 kV and 40 mA, equipped with a PS detector with amplitude of 2.113° located at the CCiTUB. Patterns were obtained by scanning random powders from 4° to 80° (2θ) on samples crushed in an agate mortar to a particle size below 40 μm or on oriented mounts. The oriented clay mineral aggregates were prepared by glass slide method before separating clay minerals from clasts (Moore and Reynolds, 1997). Datasets were obtained using a scan time of 50 seconds at a step size of 0.017° (2θ) and variable automatic divergence slit. Quantitative mineral phase analyses were obtained by full refinement profile using XRPD. The software used was TOPAS V4.2 (2009).

Thermal analyses were carried out by simultaneous DTA-TGA, using a Netzsch instrument (STA 409C model) located at the Department of Mineralogy, Petrology and Applied Geology from the Earth Sciences Faculty of the University of Barcelona (Barcelona, Catalonia, Spain). Analyses were carried out under a temperature range of 25 to 950°C, atmospheric pressure, constant flow rate of 80 mL/min, and at a heating rate of 10 °C/min in an Al_2O_3 crucible. The sample amount used was approximately 80 mg.

Major, minor, and trace elements were determined at the ACTLABS Activation Laboratories Ltd., (Ancaster, Ontario, Canada) with the analytical package ‘‘4Litho”, using fusion inductively coupled plasma emission (FUS-ICP) and inductively coupled plasma emission mass spectrometry (ICP-MS) (for details see http://www.actlabs.com).

RESULTS

Kaolin petrography

Kaolin samples are made up of soft powder with white to gray, pale yellow and pale brown colors, containing some consolidated fragments.

Particle-size distribution of Caluquembe kaolin shows that silt fraction is predominant whereas clay and sand fractions are less abundant. Therefore, 4.9 to 8.8 vol. % of kaolin particles are less than 2 µm in size; 54.1 to 75.1 vol. % between 2 µm and 63 µm; 12.6 to 17.9 vol. % between 63 µm and 125 µm; and 3.3 to 12 vol. % between 125 µm and 250 µm.

Quartz, microcline, and plagioclase (albite) are set in a finer-grained mass (groundmass) composed by muscovite and kaolinite (Figure 3a). Quartz occurs as irregular fragments of 500 µm in size with typical angular borders. Microcline anhedral grains are up to 200 µm in diameter and they are commonly altered to cryptocrystalline kaolinite. Plagioclase has grain size of less than 100 µm and is also altered to sericite. SEM-BSE images show that in the finer-grained mass, muscovite occurs as tabular habit crystals (50 µm in length) while particles of kaolinite often show a platy habit and are stacked together forming "booklets" or radial aggregates, even both phases can be also found as very fine anhedral particles (Figure 3b). Some particles of muscovite are separated by cleavage (Figure 3c). Kaolinite is also found as muscovite-kaolinite intergrowths (up to 50 µm in length), which could be distinguished using EDS microanalysis (Figure 3b). Phosphate enriched in LREE (Light Rare Earth Elements), probably monazite-(Ce), is also found an accessory mineral phase (Figure 3d).

X-ray powder diffraction (XRPD)

The quantitative analysis of 26 whole-rock random powders (XRPD) show that samples are mainly comprised of kaolinite (50.4 to 87.0 wt. %), quartz (0 to 23.5 wt. %), albite (0.3 to 7.4 wt. %), microcline (1.2 to 21.5 wt. %) and muscovite (1.1 to 29.2

wt. %) (Table 1). Scarce hematite (<1 wt. %) is also found in some samples, except in sample KP1, which contains a significant amount of accessory minerals, with 1.6 wt. % of hematite and 2.4 wt. % of calcite. The shallower samples (KA, KU3, KU6B, KKL17B, KL13-2, L-1 and L-2) are richer in kaolinite than samples obtained from base of the profiles. For instance, samples KU6B (shallow) and KU6D (deep) from the same outcrop contain 71.5 wt. % and 58.9 wt. % of kaolinite, respectively (Table 1).

XRPD profile refinement for sample KL13-2 reveals a significant percentage of kaolinite (84.2 wt. %), less than 1 wt. % of quartz, and very low muscovite content (2.9 wt. %) (Figure 4a). Sample KC12 has higher quartz (23.5 wt. %) and muscovite contents (21.3 wt. %), and less kaolinite (50.4 wt. %). A negative correlation (R^2=0.67) between the wt. % content of kaolinite and muscovite plus K-feldspar is evident in the analyzed samples (Figure 5).

The average crystallite size for kaolinite is 15-35 nm, calculated from the profile refinement by XRPD.

Five samples containing illite and three samples containing smectite were identified (Table 2). The three smectite-bearing samples (KL6E, KL8E*, and KLB10) are located in the deepest part of the outcrop, containing a low kaolinite grade (Table 2). Illite-bearing samples KK13 and KK11A also contain goethite: 12.9 wt. % and 22.9 wt. %, respectively.

The XRPD pattern of three samples show the d_{00l} of illite, muscovite, smectite, and kaolinite in the region of 4° to 15° (2θ) (Figure 6). The d_{002} band for illite at 10.03 Å was broader and less intense than that for muscovite at d_{002}= 9.97 Å. A broad and low intensity maximum for smectite is at d_{001} = 14.9 Å. The d_{001} of kaolinite at 7.14 Å shows no appreciable differences in the XRPD profile of these samples and is narrow and intense.

In the XRD pattern of oriented mounts samples is possible to distinguish kaolinite, the reflections d_{00l} disappeared after heating to 550 °C. After ethylene glycol treatment there is not variations detected. In contrast, the XRD patterns of oriented mounts of samples with smectite have significant changes. The peak at d_{001} = 14.9 Å changes to 17 Å when solvated in ethylene glycol, and changes to 10 Å when the sample is heated to 550 °C. Samples with illite show only a slight expansion of the broad reflection at d_{002} = 10.03 Å when solvated in ethylene glycol, indicating a small proportion of expanded clay (Thorez, 1975; Moore and Reynolds, 1997).

The physical properties of kaolin, such as whiteness, abrasiveness, particle size, shape and distribution, viscosity, and rheology vary depending on the genetic conditions of the deposits. Kaolinite Crystallinity Index (KCI) may be significant to the calculation of the degree of crystal perfection in kaolinite, which is a necessary parameter to evaluate kaolinite quality for industrial applications, in addition to the plasticity correlation. In the XRPD pattern, reflections 020, $1\bar{1}0$ and $11\bar{1}$ were detected in the region of 20° to 23° (2θ). These reflections are sensitive to random and interlayer displacements and allow calculating for KCI (HI from Hinckley, 1963; IK from Stoch, 1974; AGFI from Aparicio *et al*., 2006). The Hinckley crystallinity index (HI, Hinckley, 1963) is one of the most widely used indices. Normal values range from <0.5 (disordered) to 1.5 (ordered). The calculated HI index in the region of 20° to 23° (2θ) is of 1.06 in sample KA, 1.05 in sample KC12, and 1.09 in sample KL12A. The HI of Caluquembe kaolin is generally higher than reported in other kaolin deposits worldwide such as the sedimentary kaolin from Warren (Georgia, USA) with 0.56 HI or the kaolin from Montecastelo (Spain) presenting 1.00 HI (Aparicio et al. 2006). The IK index or Stoch index (Stoch, 1974) is measured in the same zone as for HI, and the normal values range from >1.0 (disordered) to <0.7 (ordered). The calculated IK index in the region of 20° to 23° (2θ) is 1.04 (disordered) in sample KL12A.

According to Aparicio and Galan (1999), the KCI can only be determined as an approximate value. Kaolinite maximums by XRPD are close to the muscovite and quartz maximums in the region of 20° to 23° (2θ) (Figure 4b and 4c). Aparicio *et al*. (2006) present a new AGFI (Aparicio-Galán-Ferrel Index) based on the additional processing to decompose overlapping peaks detected in the region of interest with the software MacDiff (Petschick, 2004).

Peak intensities of 020, $1\bar{1}0$ and $11\bar{1}$ in kaolinite has been determined through full profile refinement by XRPD and the software Topas V4.2 in samples from Caluquembe. Sample KC12 has quartz (24 wt. %) and muscovite (21 wt. %), with an AGFI of 1.35 (Figure 4b). Sample KA has <1 wt. % of quartz and 9 wt. % of muscovite, and an AGFI of 1.06 (Figure 4c). Sample KL12A has 5 wt. % of quartz and 20 wt. % of muscovite and an AGFI of 1.19. According to Aparicio *et al*. (2006), these samples can be classified as low and medium defect kaolinite. Similar data were obtained by Aparicio *et al*. (2006) in kaolinite from Mevaiela (Angola). In this case, the AGFI is 1.35 in kaolinite containing 20 wt. % of quartz, which suggests that AGFI is more accurate in determining the crystallinity of the sample and is also related to the kaolinite content.

Differential thermal and thermogravimetric analysis (DTA-TGA)

The DTA curve (Figure 7) only shows an endothermic peak in dry air conditions at 540.3 °C in sample KL132, confirming the dehydration of kaolinite (Mackenzie, 1957; Liu *et al*., 2015). Samples have a mass loss between 6.2 and 13.0 wt. % up to 650ºC in

TGA curve. Samples with higher kaolinite contents show a more significant mass loss. The amount of kaolinite calculated by mass loss is between 44.3 and 92.9 wt. % (Table 1).

Correlation between TGA and XRPD

Thermal analyses have been carried out to check the quantitative results of mineral phases calculated by XRPD using the correlation between the calculated wt. % of kaolinite in the profile refinement by XRPD and the calculated wt. % of kaolinite in TGA (Figure 8). Samples containing more kaolinite also have higher mass loss that shows a positive correlation (R^2=0.75). The model proposed demonstrates an adequate accuracy for the quantification of kaolinite and shows that material sampled closer to the surface is richer in kaolinite than samples from the deeper part of the profile. The quantitative results of samples containing illite and smectite give more inaccurate values considering that the thermal characteristics of kaolinite are influenced by the presence of smectite and illite.

Kaolin geochemistry

The average chemical composition of kaolinite determined by EMPA is: 46.28 SiO_2, 36.31 Al_2O_3, 0.58 MgO, 0.03 Na_2O, 0.10 TiO_2, 0.85 Fe_2O_3, 0.03 MnO, 0.04 BaO, 0.07 CaO, 0.05 K_2O wt. %. The average structural formula based on 14 oxygens is the following: $(Al_{3,77}Fe^{3+}_{0,05}Mg_{0,06})_{3.9}\ Si_{4,0}\ O_{10}\ (OH)_{8.}$

Major-, trace- and REE concentrations have been obtained from six representative samples from the Caluquembe area (Table 3 and 4). Two kaolin samples from Uganda (Nyakairu and Koeberl, 2001), one from Cameroon (Njoya *et al.*, 2006) and one from Sa Bandeira granite in Huambo (Angola) are also shown for comparison in Tables 3 and 4. Sa Bandeira granite has a very similar composition to the granites that outcrop in the Caluquembe area (Montenegro de Andrade, 1954).

Major elements generally show a different trend in the altered sample compared to the parent rock (Table 3). The SiO_2 trend of Caluquembe kaolin is decreasing and the Al_2O_3 trend is increasing compared to the granite from Sa Bandeira. SiO_2 is high for all samples ranging between 45.35 and 63.24 wt. %. Al_2O_3 contents lie between 21.89 and 32.24 wt. %. Fe_2O_3 is between 1.36 and 4.25 wt. %. K_2O is between 1.16 and 4.03 wt. %. TiO_2 is between 0.49 and 0.86 wt. %. Other remaining oxides (Mn, Mg, Ca, Na) are only present as traces (<0.2 wt. %). Loss on ignition (LOI) values are between 7.80 and 13.69 wt. %.

The most abundant trace elements are: Zr from 162 (sample L1) to 430 (sample K6E) ppm; Ba from 222 (sample K6E) to 1090 (sample KL13-2) ppm; Rb from 54 (sample KL13-2) to 206 (sample KLB 10) ppm. Other trace elements such as Sc, V, Cr, Co, Ni, Cu, Zn, Ga, Sr, Y, Nb, Hf, Pb, Th, and U are usually less than 100 ppm. As, Mb, Ag, In, Sn, Sb, Cs, Ta, W and Bi are less than 5 ppm (Table 4).

REE contents in kaolin samples vary from 130 ppm (sample L1) to 564 ppm (sample KL13-2). REY (REE+Y) range between 142 ppm and 624 ppm. LREE (Light Rare Earth Elements) (La, Ce, Pr, Nd, Sm, Eu) range from 524 to 122 ppm while HREE (Heavy Rare Earth Elements) (Gd, Tb, Dy, Ho, Er, Tm, Yb, Lu) range from 40 to 8 ppm (Table 4). The C1 chondrite-normalized REE plots (Figure 9a) (McDonough and Sun, 1995) are roughly parallel and characterized by negative slopes as a result of enrichment in the LREE relative to HREE. The normalization via upper Continental Crust (UCC, Rudnick and Gao, 2003) is presented in Figure 9b. In general, Caluquembe samples present flat

REE patterns with high values of HREE, which is a relative significant enrichment similar to that reported in kaolin from Warren (Georgia, USA) from heavy, light and grit fractions (Elliott *et al*. 2018). They also have a negative Sc anomaly as reported in heavy and grit mineral fractions from Warren kaolin too. Only sample L-1 from Caluquembe has a different behaviour with and Sc enrichment as light fraction from Jeffersonville Member and Buffalo Creek in Georgia, USA.

DISCUSSION

Classification of the Caluquembe deposit

Considering the little available geological information about this area, it is necessary to establish a formal classification of the Caluquembe kaolin deposit using the mineralogical and compositional data obtained in the present work.

Kaolinite from Caluquembe is generally found as finer-grained mass of particles, though also reported as muscovite-kaolinite intergrowths. Considering the results of the granulometric curve, particle size distribution of the Caluquembe kaolin shows small amounts of the fraction below 4 µm (8.7 to 13.8 vol. %), which correspond to the kaolinite that originated by alteration of potassium feldspars, while muscovite-kaolinite intergrowths may correspond to the fraction below 63 µm (74.0 to 83.9 vol. %).

The Chemical Index of Alteration (CIA) is also a very suitable parameter to determine the weathering level of feldspars and the corresponding formation of kaolin by this process (Nesbitt and Young, 1984). CIA is expressed from 0 to 100 and it is calculated using the main compositional elements of kaolin: Al, Na, K, and Ca [$CIA=Al_2O_3 /(Al_2O_3+Na_2O+K_2O+CaO)\cdot 100$]. The CIA parameters of the Caluquembe kaolin have indexes from 82 to 95 (Table 3), which are significantly high and indicate an elevated level of feldspar alteration. In addition, it is possible to distinguish changes in the CIA parameter comparing kaolin samples obtained in the same outcrop from different depths in the profile. For instance, in sample KU6B (upper level) and sample KU6D (lower level), the CIA parameter is 87 and 82 respectively, indicating a significant increase of weathering in the upper levels which is also directly related to the kaolinite content: 71.5 and 58.9 wt. %, respectively.

During intense weathering, potassium feldspar and plagioclase are destabilized and transformed to kaolinite, while sericite and muscovite are also transformed to kaolinite especially in the upper levels of the profile (Galan, 2006). This would explain why kaolinite content decreases towards the deeper parts of the weathering profile as reported in the samples from the Caluquembe area.

The concentration ratio of La/Th as well as Y/HREE may also be useful parameters to determine kaolin provenance. In the case of Caluquembe kaolin, La/Th ratio is 2.7, which is similar to values reported in upper continental crust (2.8 ±0.2), indicating a felsic source for kaolin (Taylor and McLeman, 1995). On the other hand, Y/HREE ranges from 1.2 and 1.5, indicating a similar process during kaolinization.

Eu anomalies associated to more evolved continental crust are found, for instance, in clay-rich sediments from central Uganda (Nyakairu and Koeberl, 2001), in samples from weathered granitic rocks of south China (Bao and Zhao, 2008), in samples from Sögüt from northwetern Turkey (Kadir and Kart, 2009) and in samples from residual kaolin derived from granitic rock in SE Germany (Dill, 2016). This Eu anomaly is not found in samples from Caluquembe (Figure 9, Table 4).

We consider that all these compositional and mineralogical features of the kaolin deposits from the Caluquembe area should be regarded as strong evidence indicating that they originated from the weathering of precursor granitic rocks. Therefore, kaolin deposits from Caluquembe should be classified as primary type kaolin deposits (Dill, 2016).

Economic interest

The potential extension of kaolin outcrops in Caluquembe is estimated around 20 km^2, achieving a significant thickness that ranges from 5 to 10 meters (Figure 2). At present, a further evaluation is being carried out in the area to obtain a more accurate calculation of the extension and thickness of the kaolin deposits. However, the preliminary estimation concludes that potential inferred reserves of kaolin in the Caluquembe area are estimated around 500,000,000 m^3. Although this calculation is approximate and more accurate studies are necessary, this preliminary volume would suggest that Caluquembe is a medium-size kaolin deposit, bigger than other deposits from Western Africa such as Makoro, Botswana (Ekosse, 2000).

Al_2O_3 contents of kaolin are directly related to the kaolinite percentage and are consequently considered as a significant parameter to determine kaolin quality. Caluquembe Al_2O_3 contents (21.9 to 32.2 wt. %) and SiO_2/Al_2O_3 ratio (1.28) are similar to those reported for kaolin from the Zhanjiang, Longyan and Dazhou deposits (Guangdong Province, China; Wilson *et al.*, 1997), and slightly higher than the theoretical value for kaolinite (1.16). However, Fe_2O_3 contents of Caluquembe kaolin are quite significant (1.4 to 4.3 wt. %) and they should be considered as penalizing for the potential marketing of the Caluquembe kaolin (Saikia *et al*., 2003, Lopez Galindo *et al*., 2007).

The mineralogical and chemical compositions of kaolin from Caluquembe are similar to other African kaolins. In addition, the kaolinite grade is slightly lower or similar to those found in Koutaba and Mayouom in Cameroon (Nkalih Mefire *et al*., 2015; Njoya *et al*., 2006), central Uganda (Nyakairu *et al*., 2001), Makoro in Botswana (Ekosse, 2000) and Grahamstown in South Africa (Heckroodt, 1991) (Table 5). The mineralogical composition of three classical kaolin deposits developed from precursor granites is presented for comparison in the Table 5: Guandong (China), Otovice (Czech Republic) and Cornwall (England.) All of them have higher kaolinite contents than the Caluquembe deposit.

Considering the main features of Caluquembe kaolin, the suitable application of this material should be focused on the fabrication of bricks, pavers, roofing tiles and the ceramics industry (Heckroodt, 1991; Gomes *et al*., 1994; Savianno *et al*., 2005; Ekosse, 2000; Nyakairu *et al*., 2001; Njoya *et al*., 2006; Ekosse, 2010 ; Nkalih Mefire *et al*., 2015).

In addition, kaolin deposits have recently been considered non-conventional sources of critical metals such as REE (Aagaard, 1974; Laufer et al., 1984; Xiao et al., 2016; Sanematsu and Watanabe, 2016; Elliot et al., 2018). Values of ∑REE (La, Ce, Pr, Nd, Sm, Eu, Gd, Tb, Dy, Ho, Er, Tm, Yb, Lu) in Caluquembe are highly erratic 129.58 ppm to 563.5 ppm, Table 4 and do not show a correlation with SiO_2, Fe_2O_3, CaO, P_2O_5 and MnO. Samples are more enriched in LREE (Table 4) and the ratio LREE/HREE is homogeneous by a mean factor ~ 14. A good positive correlation exists between Y and REE (R^2=0.98) and between Y and HREE (R^2=0.99). The correlation between REY and kaolinite wt. % is positive (R^2=0.75) except in sample L-1. A positive correlation is shown between Y and kaolinite wt. % (R^2=0.78) for except sample L-1. In some samples from the Caluquembe area, the REY content is higher than 600 ppm (Table 4), which is higher than that reported in other deposits, for instance, in Uganda and Cameroon (Table 4). Therefore, considering the medium size of the Caluquembe kaolin deposit (Sanematsu and Watanabe, 2016) this can be considered as a potential non-conventional source of REY. However, more detailed studies will be necessary to determine which mineral phases are enriched in REE and their relationship between the kaolinite contents and the corresponding potential extraction of REY as a subproduct during kaolinite exploitation.

CONCLUSIONS

The present work is the first study of the recently discovered kaolin deposit from the Caluquembe area (Angola).

The studied kaolin samples do not have significant compositional and mineralogical differences. Kaolinite contents calculated from full profile refinement by XRPD range between 50.4 and 87.0 wt. % and between 44.3 and 92.9 wt. %, calculated with TGA (Figure 8). The samples that outcrop in shallower areas are richer in kaolinite than deeper samples. A relevant conclusion of the present work is that full profile fitting by XRPD and TGA results have a good correlation, and the combination of both techniques is suitable to determine kaolinite contents in this type of clay deposits.

Mineralogy and compositional features of kaolin samples indicate that Caluquembe deposits were generated by weathering of granitic rocks and the corresponding alteration of feldspars. Therefore, they should be classified as primary kaolin deposits.

The economic importance of these deposits is considered to be very relevant, especially considering that they are located in an underdeveloped region. The mineralogical and compositional features of the Caluquembe kaolin and its low to medium crystallinity indicate that the most suitable application for this clay is the manufacture of structural products, such as bricks, pavers and roofing tiles. Caluquembe kaolin would need to be refined and processed to be used in other applications, such as in the pharmaceutical industry or in the production of paper and cosmetics.

The chondrite-normalized rare earth element (REE) patterns show enrichment in the light REEs, absence of an Eu anomaly and a positive correlation has been found between kaolinite wt. % and REY content. Upcoming studies will be necessary to characterize REY contents and REY carrier mineral phases, however, their evaluation as a sub product in a possible future kaolinite exploitation is highly recommended.

Due to the high content of kaolinite in the deposit of Caluquembe, this area is very suitable for the exploration and potential exploitation of kaolinite, a very valuable raw material with a bright future.

ACKNOWLEDGMENTS

This research was supported by the CGL2012-36263, CGL2006-12973 and CGL2009-13758 projects of the *Ministerio de Ciencia e Innovación* of the Spanish Government, the AGAUR 2014SGR01661 project of the *Generalitat de Catalunya* and by a FI grant to J. Xu (coded FI_B 00904) sponsored by the *Secretaria d'Universitats i Recerca* of the *Departament d'Economia i Coneixement* of the *Generalitat de Catalunya*. The authors thank the Scientific and Technical Centers of the University of Barcelona (CCiTUB) for their support in carrying out experimental analyses.

REFERENCES

Aagaard, P. (1974) Rare earth elements adsorption on clay minerals. *Bulletin du groupe français des argiles*, **26**, 193-199.

Aparicio, P. and Galan, E. (1999) Mineralogical interference on kaolinite crystallinity index measurements. *Clays and Clay Minerals*, **47**, 12-27.

Aparicio, P., Galan, E. and Ferrell, R.E. (2006) A new kaolinite order index based on XRD profile fitting. *Clay Minerals*, **41**, 811–817.

Ashwal, L.D., Twist, D. (1994) The Kunene complex, Angola/Namibia: a composite massif-type anorthosite complex. *Geological Magazine*, **131**, 579-591.

Bailey, S.W. (1980) Structure of layer silicates. Pp. 1-123 in: *Crystal structure of Clay Minerals and their X-ray Identification* (G.W. Brindley and G. Brown, editors). Monograph, **5**. Mineralogical Society, London.

Bao, Z. and Zhao, Z. (2008) Geochemistry of mineralization with exchangeable REY in the weathering crusts of granitic rocks in South China. *Ore Geology Reviews*, **13,** 519-535.

Bish, D.L. (1993) Rietveld refinement of the kaolinite structure at 1.5 K. *Clays and Clay Minerals*, **41**, 738-744.

Bermúdez-Lugo, O. (2014) Angola and Namibia, Minerals years book. U.S. Geological Survey.

De Carvalho, H., Tassinari, C., Alves, P., Guimaraes, F., Simoes, M.C. (2000) Geochronological review of the Precambrian in western Angola: Lings with Brazil. *Journal of African Earth Sciences*, **31**, 383-402.

Detellier, C. and Schoonheydt, R.A. (2014) From Platy Kaolinite to Nanorolls. *Elements*, **10**, 201-206.

Dedzo, G.K. and Detellier, C. (2016) Functional nanohybrid materials derived from kaolinite. *Applied Clay Science*, **130**, 33-39.

Dill, H. G. (2016) Kaolin: Soil, rock and ore. From the mineral to the magmatic, sedimentary and metamorphic environments. *Earth-Science Reviews*, **161**, 16-129.

Ekosse, G-I (2000) The Makoro kaolin deposit, southeastern Botswana: its genesis and possible industrial applications. *Applied clay science*, **16**, 301-320.

Ekosse, G-I. (2010) Kaolin deposits and occurrences in Africa: Geology, mineralogy and utilization. *Applied Clay Science*, **50**, 212-236.

Elliot. W.C., Gardner, D.J., Malla, P., Riley, E. (2018) A New Look at the Occurrences of the Rare-Earth Elements in the Georgia Kaolins. *Clays and Clay Minerals*, **66** (3), 245-260.

Flanagan, M.D. (2016) *Clays in Mineral Commodity summaries*. U.S. Geological Survey, **50**.

Galán, E. (2006) Genesis of clay minerals Pp 1129-1162 in Handbook of clay science. (Bergaya, F.; Theng, B.K.G. and Lagaly, G. editors) Developments in clay science 1. Elsevier.

Galán, E., Aparicio, P., Fernández-Caliani, J.C., Miras, A., G.Márquez, M, Fallick, A. and Clauer, N. (2016) New insights on mineralogy and genesis of kaolin deposits:The Burela kaolin deposit (Northwestern Spain). *Applied Clay Science*, **131**, 14-26.

Gomes, C., Velho, J.A. and Guimaraes F. (1994) Kaolin deposit of Mevaiela (Angola) alteration product of anorthosite: assessment of kaolin potentialities for applications in paper. *Applied Clay Science*, **9**, 97-106.

Guggenheim, S., Adams, J.M., Bain, D.C., Bergaya, F., Brigatti, M.F., Drits, V.A., Formoso, M.L.L., Galán, E., Kogure, T. and Stanjek, H. (2006) Summary of recommendations of nomenclature committees relevant to clay mineralogy: report of the Association Internationale pour l'etude des Argiles, nomenclature committee for 2006. *Clay Minerals*, **41**, 863-877.

Hanson, R.E. (2003) Proterozoic geochronology and tectonic evolution of southern Africa. *In:* Yoshida, M., Windley, B.F, Dasgupta, S (eds). Proterozoic East Gondwana: Supercontinent Assembly and Breakup. Geological Society of London, Special Publications, **206**, 427-463.

Heckroodt, R.O. (1991) Clay and clay materials in South Africa. *Journal of the south African institute of mining and metallurgy,* **91**, 343-363.

Hinckley, D.N. (1963) Variability in "crystallinity" values among the kaolin deposits of the coastal plain of Georgia and South Carolina. *Clays and Clay Minerals*, **11**, 229-235.

Jelsma, H., Perrit, S.H., Armstrong, R.A., Ferreira, H.F. (2011) SHRIMP U-Pb zircon geochronology of basement rocks of the Angolan Shield, western Angola. In: *Proceedings of the 23rd CAG, Johannesburg.* Council for Geoscience, Pretoria 203.

Kadir, S. and Kart, F. (2009) The occurrence and origin of the Sögüt kaolinite deposits in the Paleozoic Saricayaka granite-granodiorite complexes and overlying Neogene sediments (Bilecik, northwestern Turkey). *Clays and clay Minerals*, **57**, 311-329.

Laufer, F., Yariv, S. and Steinberg, M. (1984) The adsorption of quadrivalent cerium by kaolinite. *Clay Minerals*, **19**, 137-149.

Liu, X., Liu*, X. and Hu, Y. (2015) Investigation of the thermal behaviour and decomposition kinetics of kaolinite. *Clay Minerals*, **50**, 199–209

López-Galindo, A., Viseras, C. and Cerezo, P. (2007) compositional, technical and safety specifications of clays to be used as pharmaceutical and cosmetic products. *Applied Clay Science*, **36**, 51-63.

MacKenzie, R.C. (1957) *The Differential Thermal Investigation of Clays*. Mineralogical Society (Clay Minerals Group), London, 456 pp.

Mansa, R., Ngassa Piegang, G. B. and Detellier, C. (2017) Kaolinite aggregation in book-like structures from non-aqueous media. *Clays and Clay Minerals,* **65**, 193–205.

Marques, M. M. (1977) Esboço das grandes unidades geomorfológicas de Angola (2ª aproximação). Instituto de Investigaçao Cientifica Tropical, Garcia de Orta, Sérvicio Geologico, Lisboa, **2(1)**, 41-43.

Mayer, A., Hofmann, A.W., Sinigoi, S., Morais, E. (2004) Mesoproterozoic Sm-Nd and U-Pb ages for the Kunene Anorthosite Complex of SW Angola. *Precambrian Research*, **133**, 187-206.

McCourt, S., Armstrong, R.A., Jelsma, H., Mapeo, R.B.M. (2013) New U-Pb SHRIMP ages from the Lubango region, SW Angola: insights into the Palaeoproterozoic evolution of the Angolan Shield, southern Congo Craton, Africa. *Journal of the Geological Society of London*, **170**, 353-363.

McDonough, W.F. and Sun, S.S. (1995) The composition of the earth. *Chemical Geology*, **120**, 223-225.

Montenegro de Andrade, M. (1954) *Rochas graníticas de Angola*. Memórias, série geológica IV. Ministério do Ultramar, 464 pp.

Moore, D.M. and Reynolds, R.C.Jr. (1997) *X-Ray Diffraction and the Identification and Analysis of Clay Minerals*. Oxford University Press, 332 pp.

Murray, H.H. (1999c) Applied clay mineralogy today and tomorrow. *Clay Minerals*, **34**, 39-49.

Murray, H.H. (2000) Traditional and new applications for kaolin, smectite, palygorskite: a general overview. *Applied Caly Science*, **17**, 207-221.

Nesbitt, H.W. and Young, G.M. (1984) Prediction of some weathering trends of plutonic and volcanic rocks based on thermodynamic and kinetic considerations. *Geochimica and Cosmochimica Acta*, **48**, 1523-1534.

Nkalih Mefire, A., Njoya, A., Yongue Fouateu, R., Mache, J. R., Tapon, N.A., Nzeukou Nzeugang, A., Melo Chinje, U., Pilate, P., Flament, P., Siniapkine, S., Ngono, A. and Fagel, N. (2015) Occurrences of kaolin in Koutaba (west Cameroon): Mineralogical and physicochemical characterization for use in ceramic products. *Clay Minerals*, **50**, 593–606.

Nguie, G., Dedzo, G.K. and Detellier, C. (2016) Synthesis and catalytic application of palladium nanoparticles supported on kaolinite-based nanohybrid materials. *Dalton Transactions*, 45.

Njoya, A., Nkoumbou, C., Grosbois, C., Njopwouo, D., Njoya, D., Courtin-Nomade, A., Yvon, J. and Martin, F. (2006) Genesis of Mayouom kaolin deposit (western Cameroon). *Applied Clay Science*, **32**, 125-140.

Nyakairu, G. W. A. and Koeberl, C. (2001) Mineralogical and chemical composition and distribution of rare earth elements in clay-rich sediments from central Uganda. *Geochemical Journal*, **35**, 13-28.

Nyakairu, G. W. A., Koeberl, C. and Kurzweil, H. (2001) The Buwambo kaolin deposit in central Uganda: Mineralogical and chemical composition. NOTE, *Geochemical Journal*, **35**, 245-256.

Petschick, R. (2004) *MacDiff* 4.2.5. http://servermac.geologie.uni-frankfurt.de/Rainer.html.

Phipps, J.S. (2014) Engineering minerals for performance applications: an industrial perspective .*Clay Minerals*, **49**, 1–16

Pruett, R.J. (2016) Kaolin deposits and their uses: Northern Brazil and Georgia, USA. *Applied Clay Science*, **131**, 3-13.

Rudnick, R.L. and Gao, R. (2003) Composition of the continental crust. Pp. 1-64 in: The Crust (R.L. Rudnick, editor). Treatise of Geochemistry, 3. Elsevier-Pergamon, Oxford, UK.

Saikia, N., Bharali, D., Sengupta, P., Bordolo, D., Goswamee, R., Saikia, P. and Borthakur P.C. (2003) Characterization, beneficiation and utilization of a kaolinite clay from Assam, India. *Applied Clay Science*, **24**, 93-103.

Sanematsu, K. and Watanabe, Y. (2016) Characteristics and Genesis of Ion Adsorptio-Type Rare Earth Element Deposits. *Reviews in Economic Geology*, **18**, 55-79.

Savianno, G., Violo, M., Pieruccini, U., lopes da Silva, E.T. (2005) Kaolin deposits from the northern sector of the Cunene Anorthosite Complex (southern Angola). *Clays and Clay Minerals*, **53**, 674-685.

Schroeder, P.A. and Erickson, G. (2014) Kaolin: From Ancient Porcelains to Nanocomposites. *Elements*, **10**, 177–182.

Silva M.V.S., 1973b. Carta Geologica de Angola. Folha N 207 Gungo. Scale 1:100 000.

Silva, A.T.S.F. and Simões, M.V.C. (1980/1981) Geologia da região de Caluquembe (Angola), *Livro de Homenagem ao Professor Doutor Carlos Teixeira pela sua jubilação, Bol. Soc. Geol. Portugal*, **22**, 363-375.

Stoch L. (1974) *Mineraly Ilaste ('Clay Minerals')*. Geological Publishers, Warsaw, 186-193.

Taylor, S.R. and McLennan, S.H. (1995) The geochemical evolution of the continental crust. *Reviews of Geophysics*, **33**, 241-265.

TOPAS (2009) *General Profile and Structure Analysis Software for Powder Diffraction Data,* version 4.2, Bruker AXS Gmbh, Karlsruhe, Germany, 2009.

Thorez, J. (1975) *Phyllosilicates and clay minerals. A laboratory handbook for their X-ray diffraction analysis*. Lelotte (Disno), France, 580 pp.

Wilson J.R., Halls, C. and Spiro, B. (1997) A comparison between the China clay deposits of China and Corwall. Proceedings of the Usher Society, **9**, 195-200.

Xiao, Y., Huang, L., Long, Z.,Feng, Z. and Wang, L. (2016) Adsorption ability of rare earth elements on clay minerals and its practical performance. *Journal of rare earths*, **34,** 5, 543-548.

Young, R.A. and Hewat, A.W. (1988) Verification of the triclinic crystal structure of kaolinite. *Clays and Clay Minerals*, **36**, 225-232.

FIGURE CAPTIONS

Figure 1. (a) Simplified geological map of Angola (Silva, 1973b); (b) Geological map the Caluquembe region and location of the studied samples.

Figure 2. Views of kaolin outcrops from the Caluquembe area: (a) Plain areas with typical surface alteration due to significant iron contents; (b), (c) and (d) kaolinite outcrops in rivers and creeks of the Caluquembe area.

Figure 3. Backscattered electron images (SEM-BSE) of sample Q-2: (a) quartz (Qtz) and feldspars (Fsp) settled in a finer-grained mass consisting of kaolinite (Kln) and muscovite; (b) Intergrowths of kaolinite (Kln) and muscovite (Ms) scattered in a groundmass comprised of kaolinite; (c) Muscovite (Ms) layers separated along cleavage surfaces; (d) REE phosphate and K-feldspars (Fsp) in a groundmass made up of kaolinite (Kln) forming booklets that are often radial.

Figure 4. (a) XRPD profile refinement (by Topas V4.2 software) of sample KL13-2. The red line corresponds to the calculated profile while the blue line corresponds to the experimental profile. The Bragg positions of mineral phases are shown at the bottom, Rwp= 8.7 (agreement with weighted profile factor in the Rietveld method); (b) XRPD profile refinement of sample KC12 in the region 17º-30º 2Θ. The blue thick line corresponds to the experimental XRD profile of this sample. The green line corresponds to the calculated XRD profile of kaolinite and d-spacing for 020 reflection for kaolinite is 4.4719Å, for $1\bar{1}0$ is 4.3649Å and for $11\bar{1}$ is 4.1803Å. The blue and purple lines correspond to calculated XRD profiles of quartz and muscovite, respectively, also included the calculated XRD profiles of hematite, albite low and microcline, Rwp=14.1;

(c) XRPD profile refinement of sample KA in the region 17º-30º 2Ɵ. The blue thick line corresponds to the experimental XRD profile of this sample. The green line corresponds to calculated XRD profile of kaolinite. The d-spacing for 020 reflection of kaolinite is 4.4694Å, for $1\bar{1}0$ is 4.3628Å and for $11\bar{1}$ is 4.1795Å. The blue and purple lines correspond to calculated XRD profile of quartz and muscovite, respectively, also included the calculated XRD profiles of hematite, albite low and microcline, Rwp=11.3.

Figure 5. Relation between muscovite+K-feldspar vs. kaolinite (wt. %) calculated by XRPD profile refinement with Topas V4.2.

Figure 6. XRPD of samples in the region from 4° to 15° 2Ɵ: (a) KL13-2, muscovite and kaolinite; (b) KL6E muscovite, kaolinite, and smectite; (c) KK8, muscovite, kaolinite, and illite.

Figure 7. DTA-TGA curves of kaolin from Calumquembe of sample KL13-2. DTA (black line) - TGA (gray line).

Figure 8. Kaolinite content (wt. %) calculated by XRPD with Topas V4.2 vs. kaolinite content (wt. %) calculated by mass loss in TGA.

Figure 9. The enrichment/depletions of REE of Caluquembe kaolin samples: a) Results normalized to C1 chondrite (McDonough and Sun, 1995); b) Results normalized to UCC (Rudnick and Gao, 2003).

TABLES

Table 1. Mineral content (wt. %) calculated by XRPD profile refinement with Topas V4.2. Temperature of dehydration (Tm) of kaolinite, mass loss and kaolinite content (wt. %) calculated by TGA.

Table 2. Mineral content (wt. %) calculated by XRPD profile refinement with Topas V4.2 in samples with smectite and illite. Temperature of dehydration (Tm) of kaolinite, mass loss and kaolinite content (wt. %) calculated by TGA.

Table 3. Major elements composition of kaolin samples (wt.%) from Caluquembe, Angola; sample BW-1 from Buwambo, and MG-1 from Migade, Uganda (Nyakairu *et al*., 2001); sample MY03 from Mayouom, Cameroon (Njoya *et al*., 2006); granite from Sa Bandeira, Angola (Montenegro de Andrade, 1954).

Table 4. Trace and REE elements (ppm) of samples from Caluquembe, Angola; sample BW-1 from Buwambo, and MG-1 from Migade, Uganda (Nyakairu et al., 2001); sample MY03 from Mayouom, Cameroon (Njoya et al., 2006). n.d =not detected, <dl= <to detection limits

Table 5. Mineralogical composition determined by XRPD (wt.%) of different kaolin deposits from Africa (Angola, Cameroon, Uganda, South Africa, Botswana) and worldwide (China, Czech Republic and England).

Figure 1

Click here to access/download;Figure;Fig_1.jpg

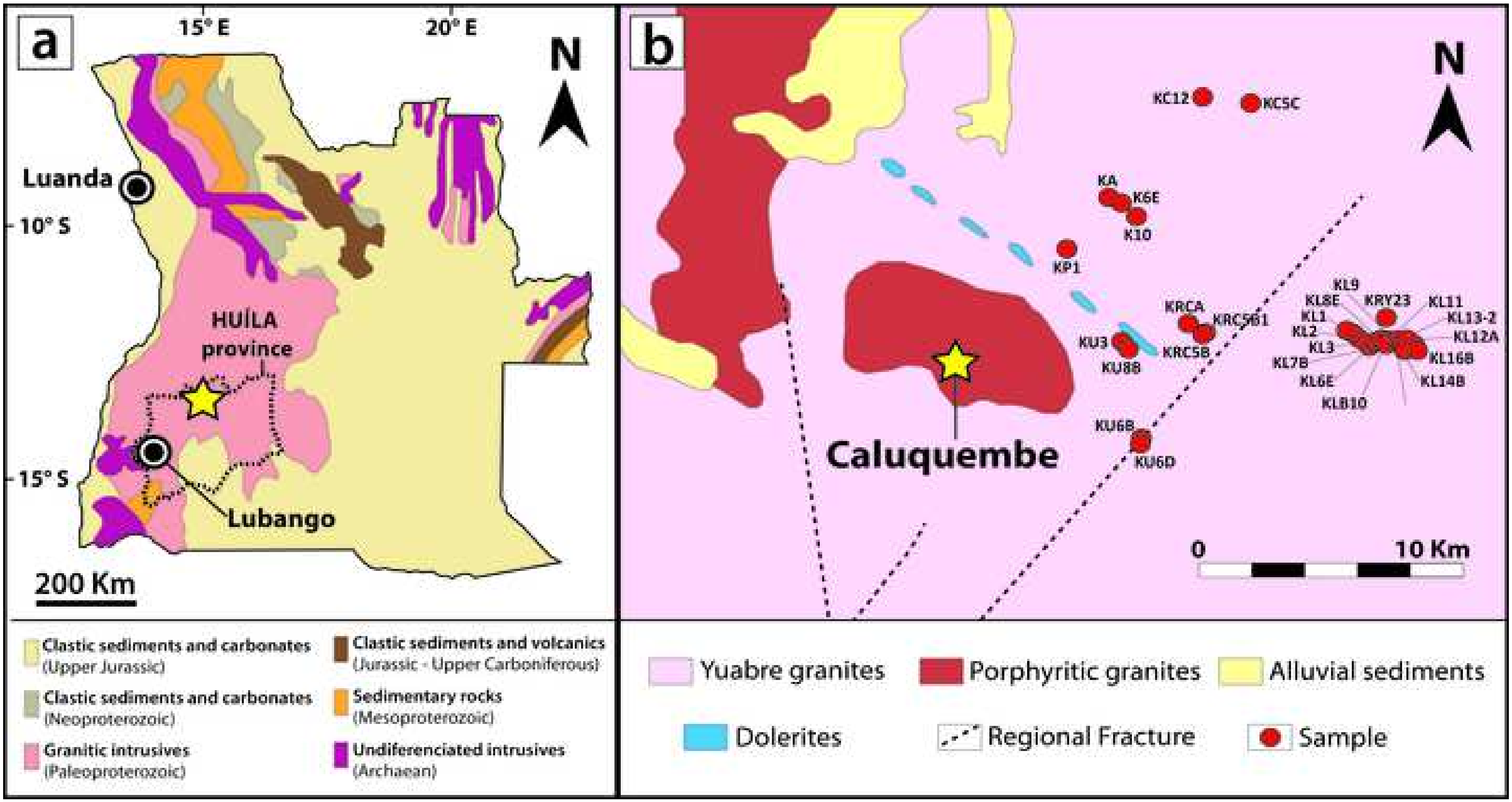

Figure 2

Click here to access/download;Figure;Fig_2.jpg

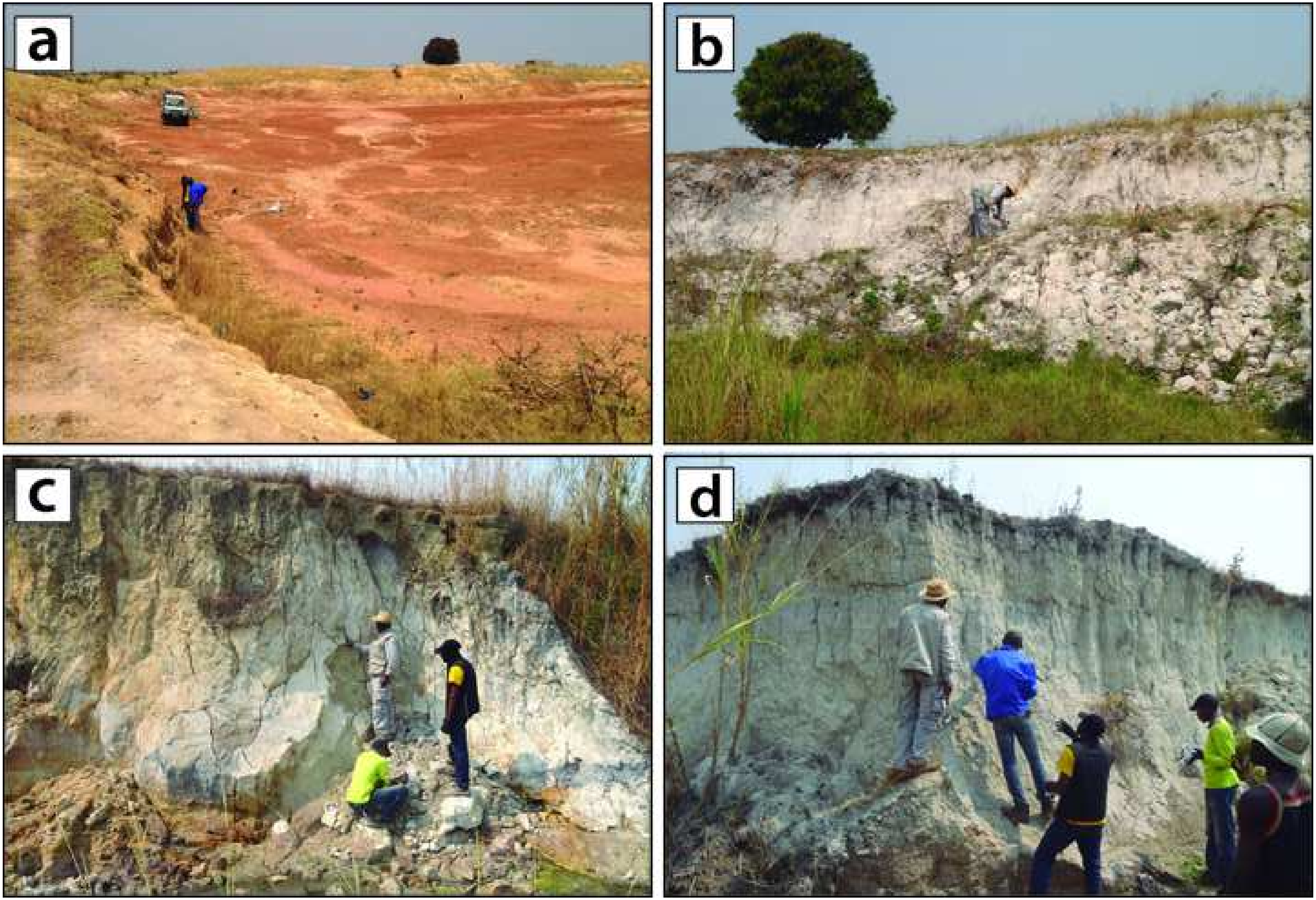

Figure 3

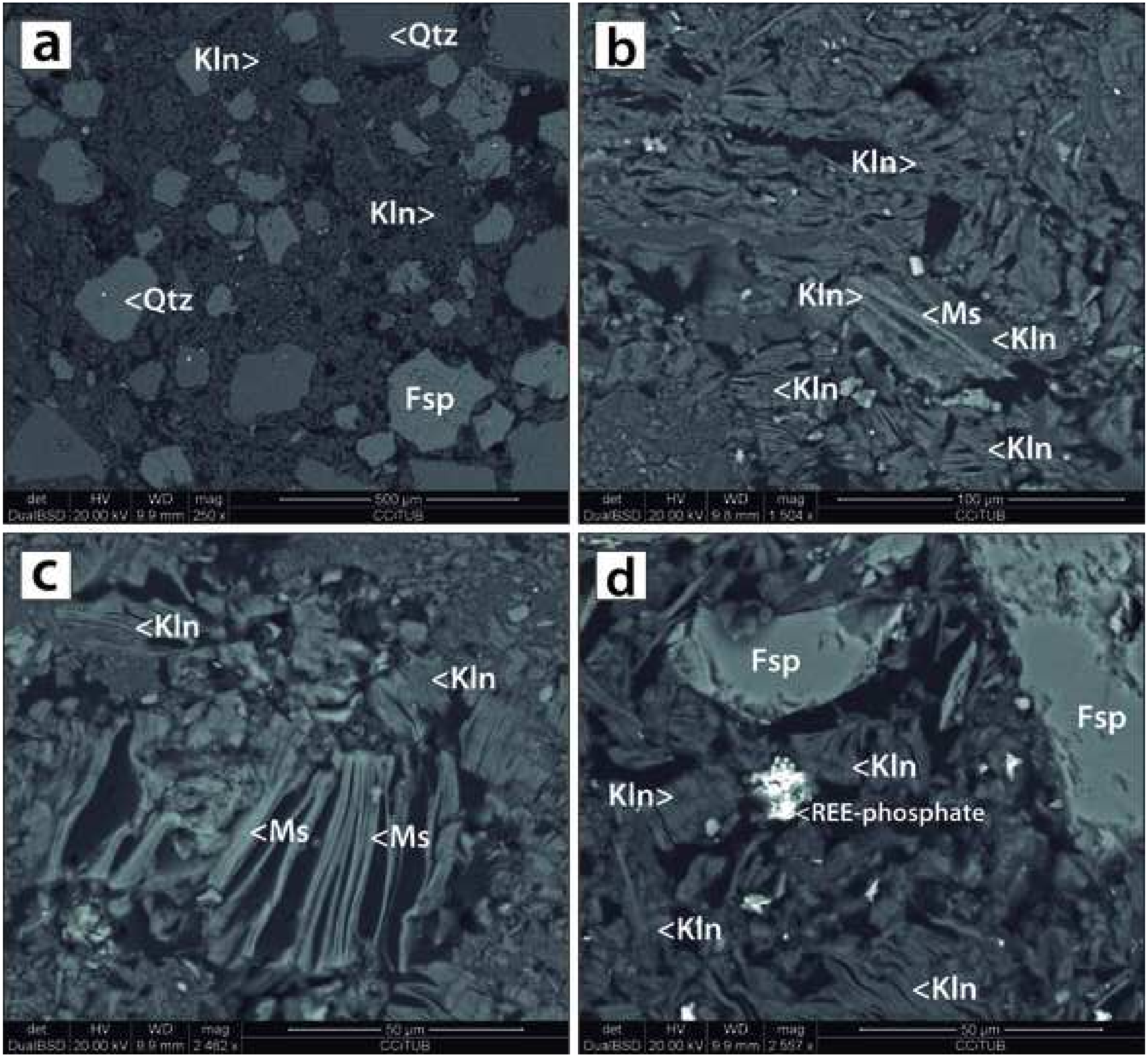
a
<Qtz
Kln>
Kln>
<Qtz
Fsp
500 µm
b
Kln>
Kln>
<Ms
<Kln
<Kln
<Kln
100 µm
c
<Kln
<Kln
<Ms
<Ms
50 µm
d
Fsp
Fsp
<Kln
Kln>
<REE-phosphate
<Kln
<Kln
50 µm

Figure 4

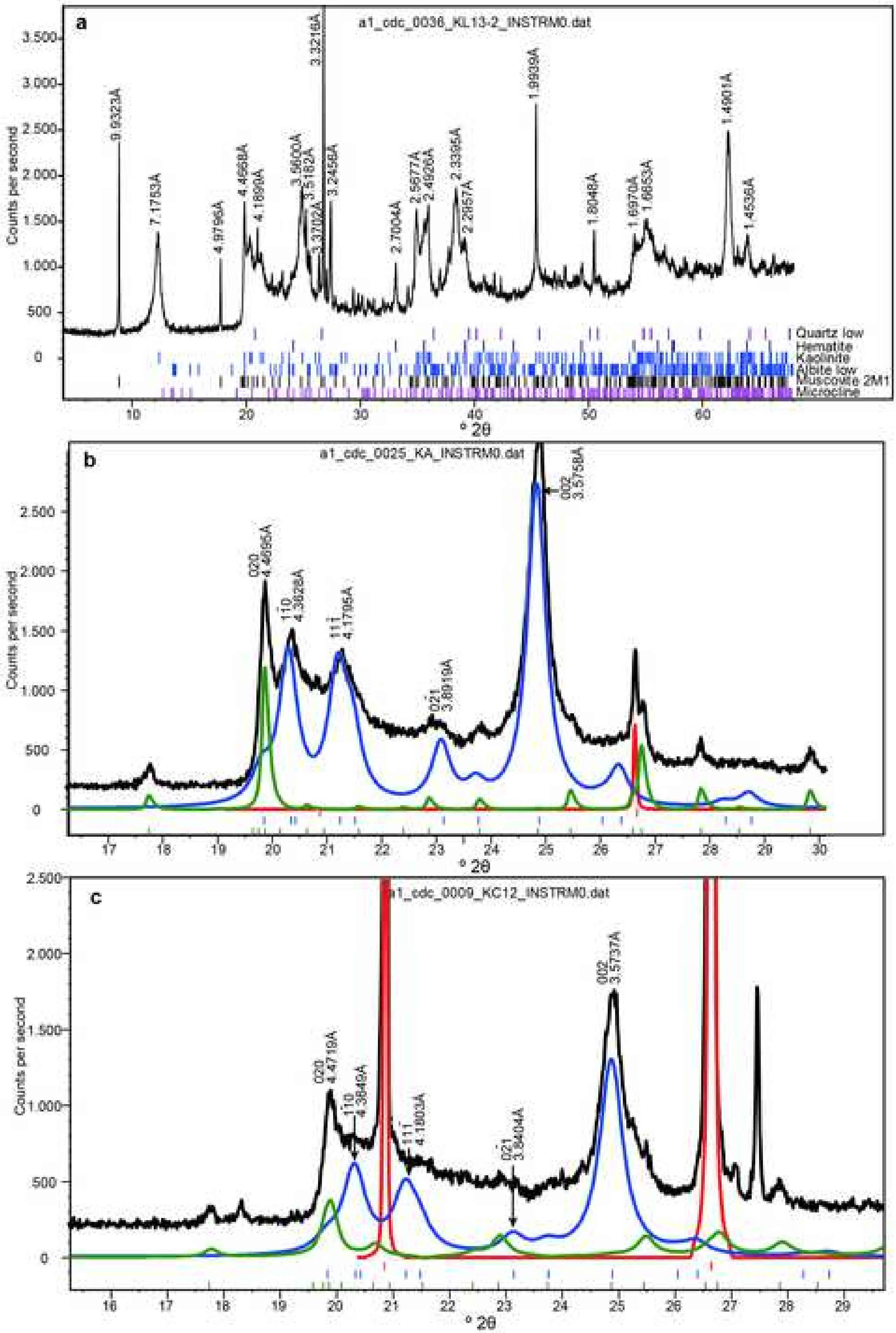
a
a1_cdc_0036_KL13-2_INSTRM0.dat
Counts per second
° 2θ
Quartz low
Hematite
Kaolinite
Albite low
Muscovite 2M1
Microcline
b
a1_cdc_0025_KA_INSTRM0.dat
c
a1_cdc_0009_KC12_INSTRM0.dat

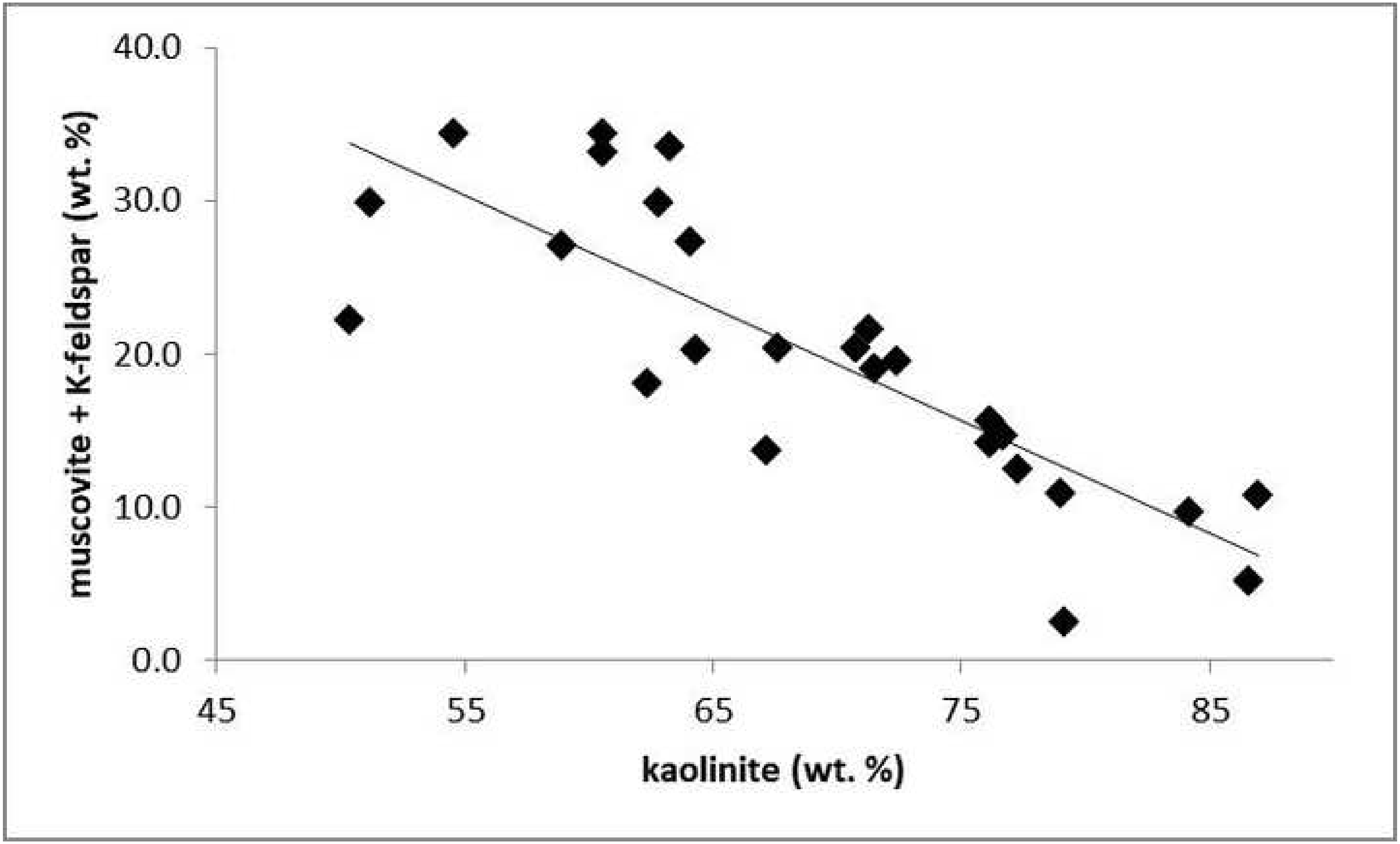
40.0
30.0
20.0
10.0
0.0
muscovite + K-feldspar (wt. %)
45
55
65
75
85
kaolinite (wt. %)

Figure 6 Click here to access/download;Figure;Fig_6.jpg

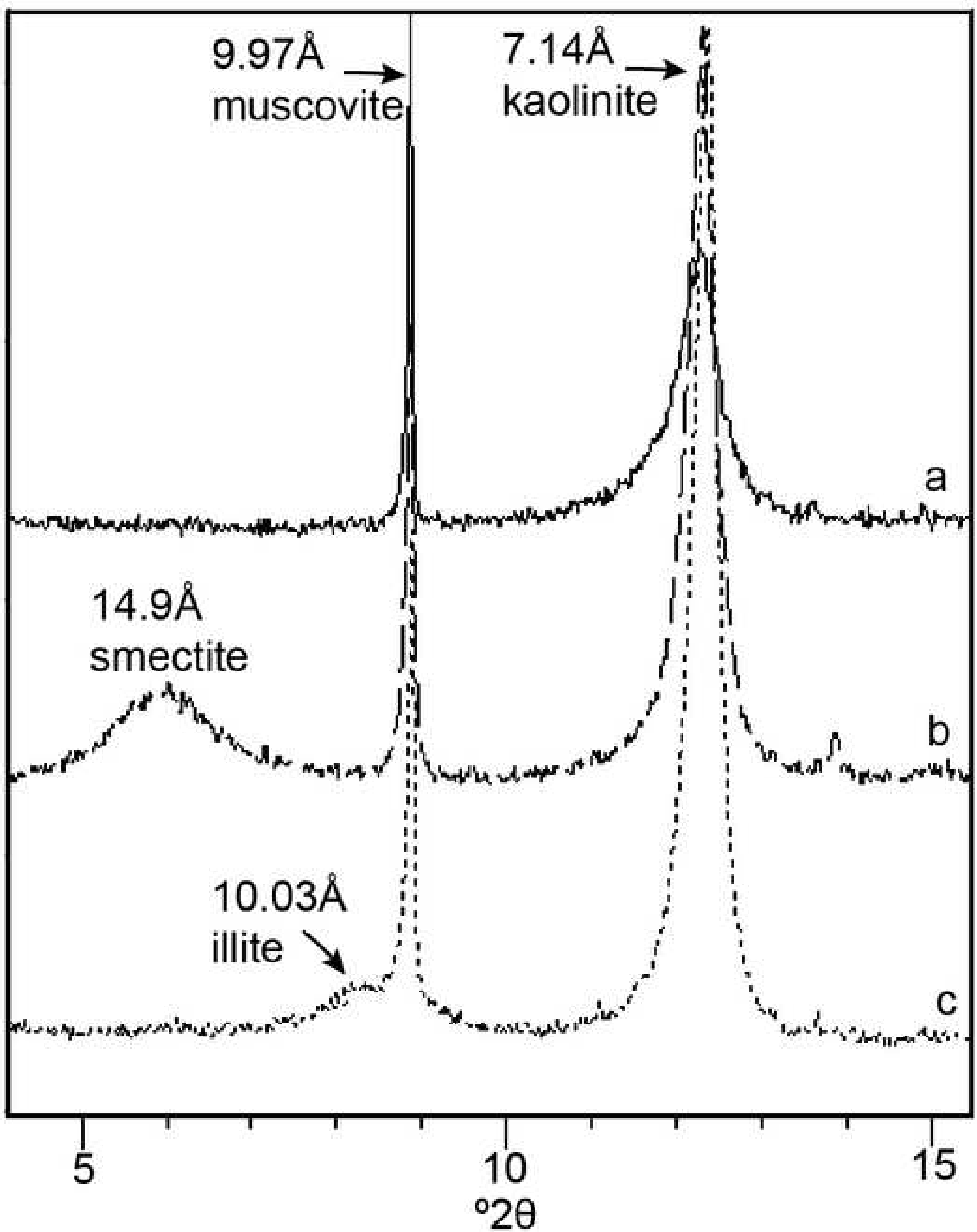

Figure 7

Click here to access/download;Figure;Fig_7.jpg

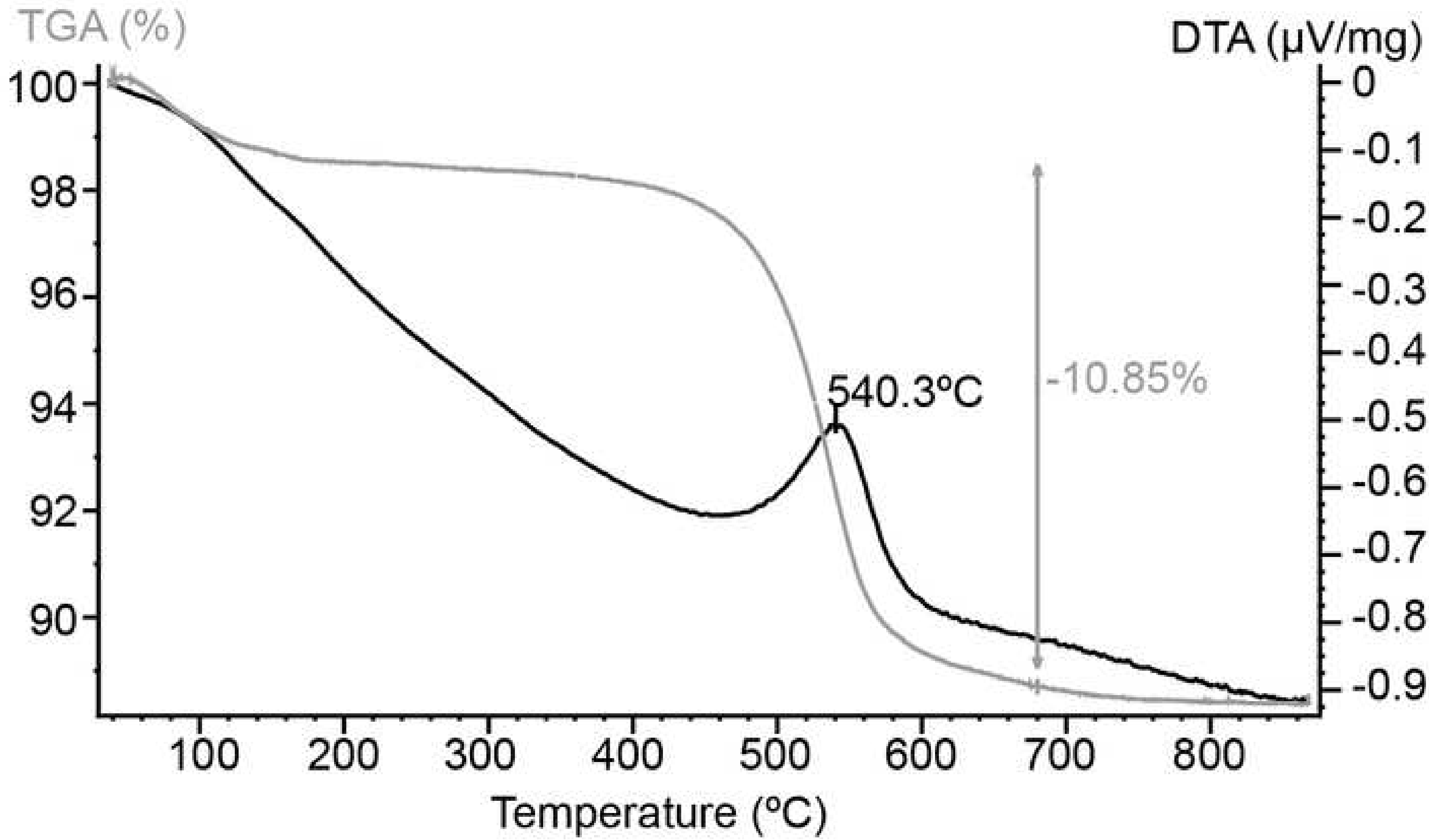

Figure 8

Click here to access/download;Figure;Fig_8.png

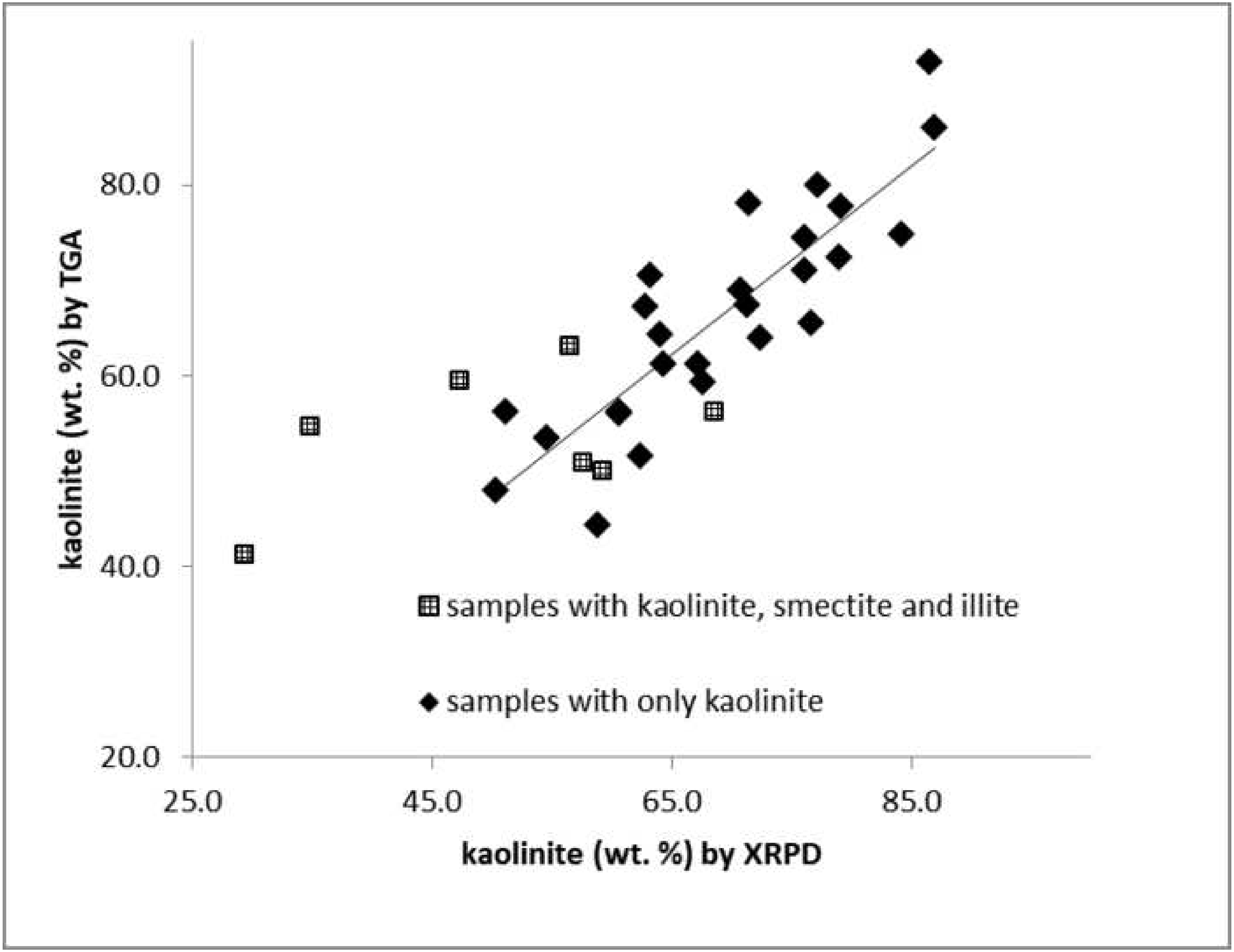

Figure 9 Click here to access/download;Figure;Fig_9jpg.jpg

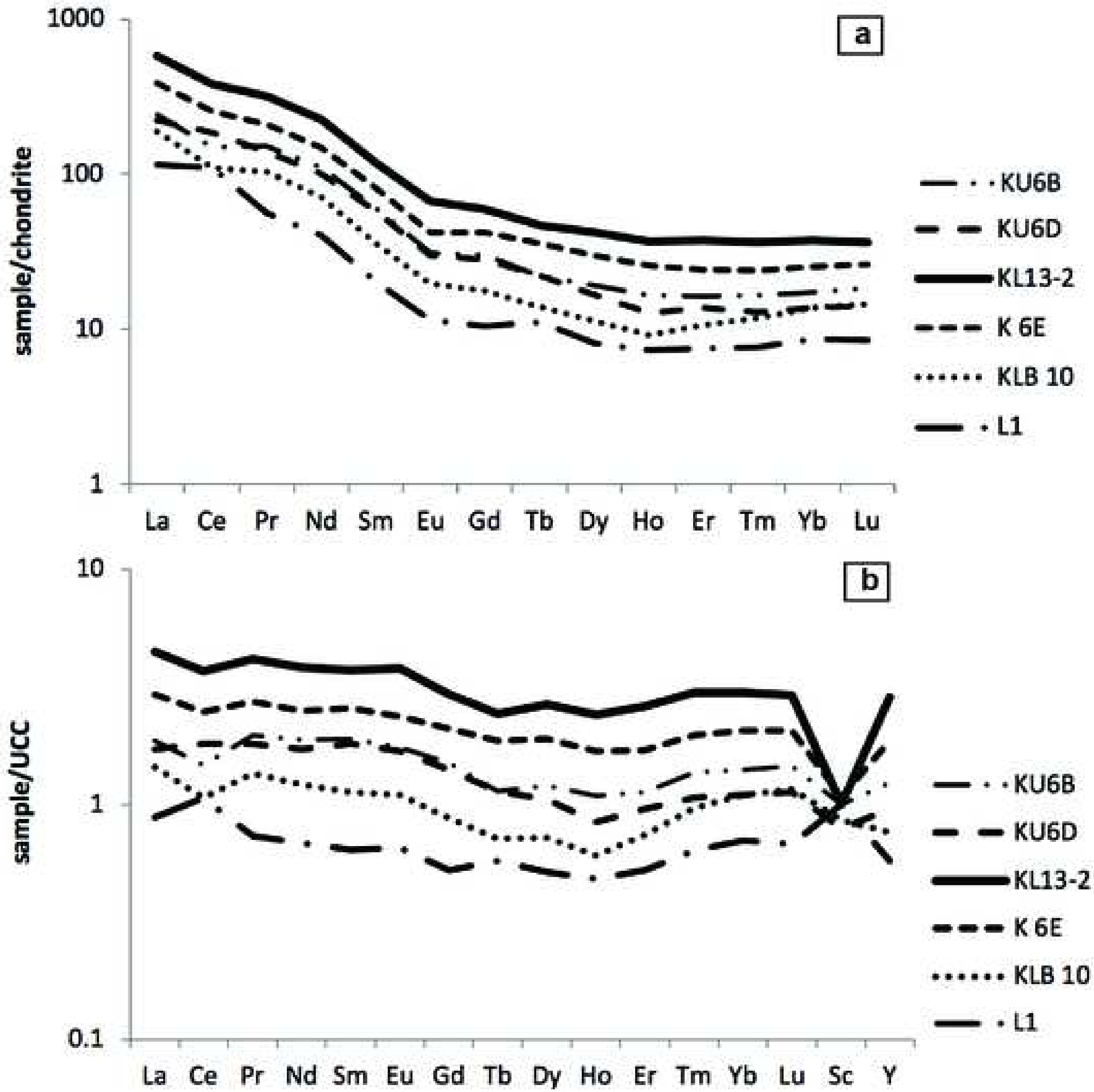

	Full profile refinement XRPD (wt. %)					
Sample	kaolinite	muscovite	quartz	plagioclase	microcline	hematite
KA	87	8.6	0.3	2	2.1	0.02
K6E	67.2	10.7	13.1	5.9	3	0.06
K10	64.3	17	10.1	5.3	3.2	0.05
KP1	70.8	8.5	2.8	1.97	11.9	1.6
KC12	50.4	21.3	23.5	3.8	0.9	0.07
KC5 C	51.2	27.3	11.5	7.4	2.6	0.04
KU3	79.2	1.1	14.8	2.9	1.4	0.58
KU6B	71.5	3.9	7.7	1.8	15.1	0
KU6D	58.9	5.5	10.5	3.6	21.5	0.04
KU8B	54.6	24.6	8.8	2.1	9.8	0.07
KRC3B	63.3	21.4	2.9	0.3	12.1	0.03
KRC5B	62.8	23.9	3.5	3.9	5.9	0.04
KRC5B1	64.1	20.8	4	4.6	6.5	0.03
KRY23	76.7	9.9	7.7	0.9	4.8	0.03
KRCA	77.3	8.4	5.7	4.5	4.1	0.04
KK14C	60.6	29.2	4.3	0.3	5.1	0.5
KKL13B	71.3	17.2	5.3	1.7	4.4	0.06
KKL17B	76.2	11.5	4.2	4	4.1	0.04
KL9	62.4	12.4	15.1	4.3	5.7	0.11
KL11	67.6	14.9	10.2	1.7	5.5	0.06
KL12A	76.2	11.2	4.8	4.7	3	0.06
KL13-2	84.2	2.9	0	5.7	6.7	0.5
KL14B	60.6	26	5.1	1.2	7.1	0.02
KL16B	72.4	15.4	5.3	2.6	4.1	0.2
L-1	86.6	3.9	1.9	6.3	1.2	0.1
L-2	79	7.3	6.9	3.2	3.6	0.01

Tm (ºC)	TGA Mass loss (wt.%)	kaolinite (wt. %)
550.3	12.0	85.9
531.0	8.6	61.1
529.3	8.6	61.1
539.1	9.7	68.9
518.7	6.7	47.9
530.4	7.9	56.2
526.6	10.9	77.6
531.4	10.9	78.0
520.0	6.2	44.3
530.1	7.5	53.4
542.4	9.9	70.4
540.8	9.4	67.2
541.0	9.0	64.3
532.3	9.2	65.5
546.0	11.2	80.0
528.3	7.9	56.2
534.2	9.4	67.4
541.8	10.4	74.4
525.4	7.2	51.5
537.6	8.3	59.2
536.0	10.0	71.0
540.3	10.5	74.8
541.6	7.8	56.0
537.2	9.0	64.0
527.9	13.0	92.9
518.4	10.1	72.4

	Full profile refinement XRPD (wt.%)					
Sample	kaolinite	muscovite	illite	smectite	quartz	plagioclase
KK8	54	12	15		9	4
KK11A	57.6		8.1		5.7	2.1
KK13	59.3		7.4		9.6	2.8
KL6E	29.4	30.6		16.7	5.5	11.5
KL7B	56.5	9.9	18.4		3.8	4.8
KL8E*	34.8	23.8		15.8	4.8	6.0
KLB10	47.4	24.0		10.1	5.5	4.0
L-3	68.6	2.7	22.1		3.9	2.0

microcline	hematite	Tm (ºC)	TGA Mass loss (wt.%)	kaolinite (wt.%)
6	0	520.1	7.7	54.8
3.6	0.0	531.6	7.1	50.9
8.0	0.2	528.3	7.0	50.0
6.3	0.0	525.9	5.8	41.2
6.5	0.0	535.0	8.8	63.1
14.5	0.4	537.7	7.6	54.6
9.0	0.1	530.8	8.3	59.5
0.6	0.0	521.9	7.9	56.2

Major elements wt.%	Caluquembe Angola KU6B	Caluquembe Angola KU6D	Caluquembe Angola KL13-2	Caluquembe Angola K 6E	Caluquembe Angola KLB 10
SiO_2	53.10	63.24	45.35	56.08	51.57
Al_2O_3	27.72	21.89	31.79	26.60	27.07
TiO_2	0.57	0.49	0.86	0.79	0.69
Fe_2O_3(T)	3.58	1.54	4.15	1.36	4.25
MnO	0.02	0.01	0.18	0.01	0.02
MgO	0.52	0.31	0.50	0.17	0.80
CaO	0.13	0.15	0.18	0.09	0.08
Na_2O	0.07	0.14	0.03	0.01	0.04
K_2O	3.55	4.03	2.02	1.16	3.63
P_2O_5	0.04	0.03	0.01	0.08	0.03
LOI	10.55	7.80	13.69	12.71	10.98
Total	99.84	99.64	98.74	99.07	99.17
CIA	87	82	93	95	87

Caluquembe Angola L1	Buwambo Uganda BW-1	Migade Uganda MG-1	Mayouom Cameroon sand-p MY03	Huambo Angola Sa Bandeira
48.76	49.98	49.90	46.61	72.21
32.24	35.97	35.62	33.29	15.02
0.62	0.02	0.05	3.96	0.40
2.75	0.34	0.54	1.46	0.29
0.02	0.05	0.04	< dl	0.06
0.52	0.33	0.34	< dl	0.80
0.06	<0.010	<0.01	< dl	2.37
0.01	0.03	0.04	< dl	3.23
1.65	0.99	0.78	0.94	3.86
0.01	0.06	0.11	0.40	0.08
12.48	12.61	12.85	13.97	1.00
99.13	100.35	100.23	99.87	100.50
92	97	97	97	52

Table 4

ppm	Caluquembe Angola KU6B	Caluquembe Angola KU6D	Caluquembe Angola KL13-2	Caluquembe Angola K 6E	Caluquembe Angola KLB 10	Caluquembe Angola L1	Buwambo Uganda BW-1
Be	4	3	3	3	3	4	n.d.
V	101	69	51	54	77	74	<15
Cr	< 20	< 20	< 20	30	< 20	20	4.47
Co	6	5	10	8	7	7	1.3
Ni	< 20	< 20	< 20	< 20	< 20	< 20	19
Cu	10	< 10	50	20	50	10	52
Zn	60	50	50	50	90	60	16
Ga	36	29	42	31	34	26	n.d.
Ge	2	2	2	2	2	2	n.d.
As	< 5	< 5	5	< 5	< 5	< 5	0.12
Rb	167	155	54	113	206	130	58.3
Sr	40	41	65	20	44	22	39.1
Zr	368	281	337	430	278	162	142
Nb	18	15	22	24	14	17	6
Mo	< 2	< 2	2	< 2	< 2	< 2	n.d.
Ag	1.3	1	1.3	1.5	1	< 0.5	n.d.
In	< 0.2	< 0.2	< 0.2	< 0.2	< 0.2	< 0.2	n.d.
Sn	3	2	4	4	5	3	n.d.
Sb	< 0.5	< 0.5	< 0.5	< 0.5	< 0.5	< 0.5	n.d.
Cs	3.3	3	< 0.5	5.9	2.4	3.9	2.27
Ba	595	683	1090	222	871	307	63.2
Bi	< 0.4	< 0.4	1.5	< 0.4	< 0.4	0.6	n.d.
Hf	9.8	7.5	8.7	10.7	6.9	4.9	0.66
Ta	1.8	1.7	2.3	3.1	1.7	1.6	0.34
W	5	3	13	6	6	4	n.d.
Tl	0.8	0.7	0.5	0.6	0.9	0.5	n.d.
Pb	36	36	40	38	22	26	n.d.
Th	25.1	20.1	48.6	31.7	16.9	17.9	1.66
U	7.1	6	5.6	17.2	16.1	5.9	0.84

Migade	Mayouom
Uganda	Cameroon
MG-1	sand-p MY03
n.d.	<dl
<15	718
10.9	294
1.75	1.8
24	5.4
105	n.d.
24	43.2
n.d.	38
n.d.	1.77
0.23	n.d.
58	17.3
65.9	383
139	489
6	57.9
n.d.	4.08
n.d.	n.d.
n.d.	0.18
n.d.	3.51
n.d.	n.d.
3.61	1.01
114	644
n.d.	n.d.
0.86	11.2
0.38	4.44
n.d.	0.8
n.d.	n.d.
n.d.	9.62
1.25	6.86
1	1.75

Table 5

ppm	Angola KU6B	Angola KU6D	Angola KL13-2	Angola K 6E	Angola KLB 10	Angola L1	Uganda BW-1	Uganda MG-1	Cameroon sand-p MY03
La	57.5	53.1	138	91.3	44.6	27.4	101	215	120
Ce	92.2	114	232	156	67	67	37.5	143	243
Pr	14	12.9	29.5	19.4	9.59	5.23	n.d.	n.d.	27.3
Nd	50.8	46.2	103	67.5	32.6	18.4	51.5	159	96.5
Sm	8.9	8.5	17.5	12.1	5.3	3	9.69	15.8	20.3
Eu	1.74	1.69	3.8	2.37	1.1	0.65	2.16	2.25	5
Gd	6	5.6	11.8	8.4	3.5	2.1	5.51	4.61	17.4
Tb	0.8	0.8	1.7	1.3	0.5	0.4	0.9	0.71	2.34
Dy	4.7	4.1	10.4	7.4	2.8	2	n.d.	n.d.	12.7
Ho	0.9	0.7	2	1.4	0.5	0.4	n.d.	n.d.	2.09
Er	2.6	2.2	6	3.9	1.7	1.2	n.d.	n.d.	4.86
Tm	0.41	0.32	0.9	0.59	0.29	0.19	0.26	0.29	0.7
Yb	2.8	2.2	6	4.1	2.2	1.4	1.21	1.03	4.1
Lu	0.45	0.35	0.9	0.64	0.36	0.21	0.14	0.1	0.6
Sc	14	11	14	15	12	14	1.2	1.89	0
Y	26	20	60	39	16	12	10	8	48.3
∑REE	243.8	252.66	563.5	376.4	172.04	129.58	209.87	541.79	556.89
∑LREE	225.14	236.39	523.8	348.67	160.19	121.68	201.85	535.05	512.1
∑HREE	18.66	16.27	39.7	27.73	11.85	7.9	8.02	6.74	44.79
LREE/HREE	12.07	14.53	13.19	12.57	13.52	15.40	25.17	79.38	11.43
La/Th	2.29	2.64	2.84	2.88	2.64	1.53	60.84	172.00	17.49
Y/HREE	1.39	1.23	1.51	1.41	1.35	1.52	1.25	1.19	1.08

UCC	C1Ch.
31	0.237
63	0.613
7.1	0.0928
27	0.457
4.7	0.148
1	0.0563
4	0.199
0.7	0.0361
3.9	0.246
0.83	0.0546
2.3	0.16
0.3	0.0247
2	0.161
0.31	0.0246
14	5.92
21	0.026

Table 6 Click here to access/download;Table;TABLE 6.xlsx

	Caluquembe Angola whole rock granite	Mayouom western Cameroon sand-poor kaolin mylonite	Koutaba western Cameroon whole rock granite	Buwambo central Uganda whole rock granite	Migade Central Uganda whole rock granite	Mevaiela Angola <2 µm fraction anorthosite
kaolinite	50 to 87	76 to 85	32 to 51	82 to 94	84 to 91	≈ 100
quartz	0 to 23.5	2 to 9	32 to 52	0 to 10	5 to 10	detected
muscovite/illite	1 to 27	1 to 8	up to 12	3 to 6	3 to 5	detected
feldspars	2 to 21	n.d.	0 to 4	1 to 4	1 to 2	detected
anatase	n.d.	3.7 to 4	n.d.	n.d.	n.d.	n.d.
hematite/goethite	0 to 1.6	0.6 to 1.4	6 to 7	n.d.	n.d.	n.d.
pyrophilite	n.d.	n.d.	n.d.	n.d.	n.d.	n.d.
references	this work	Njoya et al., 2006	Nkalih Mefire et al., 2015	Nyakairu et al., 2001	Nyakairu et al., 2002	Saviano et al., 2005

Grahamstown South Africa Witteberg shale granite	Makoro southheastern Botswana whole rock arkose	Zhanjiang, Longyan, Guangdong province China granite	Otovice Czech Republic granite	Cornwall south-west England granite
20 to 70	major	96	82 to 92	81 to 93
30 to 60	minor	0 to 1	1 to 2	1 to 2
10 to 25	trace	3 to 4	4 to 16	4 to 15
5	trace	0	n.d.	n.d.
n.d.	n.d.	n.d.	n.d.	n.d.
n.d.	trace	n.d.	n.d.	n.d.
up to 35	n.d.	n.d.	n.d.	n.d.
Heckroodt, 1991	Ekosse, 2000	Wilson et al., 1997	Wilson and Jiranek, 1995	Wilson and Jiranek, 1995